Journal of Manufacturing Processes 81 (2022) 748–758

Contents lists available at ScienceDirect

Journal of Manufacturing Processes

journal homepage: www.elsevier.com/locate/manpro

Laser powder bed fusion and casting for an advanced hybrid prototype mold

Dániel Török [a,b], Béla Zink [a], Tatyana Ageyeva [a,b,*], István Hatos [c], Martin Zobač [d], Imre Fekete [c], Róbert Boros [a,b], Hajnalka Hargitai [c], József Gábor Kovács [a,b]

[a] Department of Polymer Engineering, Faculty of Mechanical Engineering, Budapest University of Technology and Economics, Műegyetem rkp. 3., H-1111 Budapest, Hungary
[b] MTA-BME Lendület Lightweight Polymer Composites Research Group, Műegyetem rkp. 3., H-1111 Budapest, Hungary
[c] Department of Materials Science and Technology, Széchenyi István University, Egyetem Tér 1., H-9026 Győr, Hungary
[d] Institute of Scientific Instruments, The Czech Academy of Sciences, Královopolská 147., CZ-612 64 Brno, Czech Republic

ARTICLE INFO

Keywords:
Hybrid manufacturing
Multi-material structure
Multiple materials
Nondestructive evaluation
Powder bed fusion (PBF)
Computer tomography

ABSTRACT

One of the factors limiting the throughput of injection molding is cooling time, which is the most significant part of the total cycle time. The cooling efficiency of molds can be considerably improved with additive manufacturing techniques. A 3D printed injection mold with conformal cooling channels reduces cooling time by 30–40 %. However, the cooling efficiency of these molds can be further improved with a multi-material approach and the use of materials with excellent thermal and mechanical properties. In this study, we propose a hybrid mold insert made of steel and copper, produced with the combination of Laser Powder Bed Fusion (L-PBF) and casting. The steel shell that contains conformal cooling channels was printed by L-PBF. Then this shell was cast with copper. We found that the hybrid mold insert we developed has lower residual cooling time and heat extraction is more uniform than the conventional printed steel insert. The developed hybrid mold insert enables a reduction of residual cooling time by 15 %.

1. Introduction

Injection molding is one of the most widely used plastic processing techniques. Due to its high initial costs, injection molding needs to justify its feasibility, which requires large production volumes. However, the recent trends of Industry 4.0 towards mass individualization require new processing approaches that offer high efficiency and flexibility simultaneously. Because of production time and costs, the bottleneck of the injection molding process is the mold itself. Designing and manufacturing a conventional mold usually takes 3 to 4 weeks, and the cost ranges from several tens to several hundreds of thousands of USD depending on the complexity, material, and the volume [1]. Bagalkot et al. [2] presented the difference in durability and production times for conventional production molds versus aluminum or additive manufacturing (AM) based molds. Galizia et al. [3] presented the evolution of molds for injection molding, from conventional molds to AM solutions. We can overcome the problem of long production time requirements by additive manufacturing (AM), which allows creating a mold within a few days or even hours at a reasonable cost.

One of the most critical issues of injection molding is cooling efficiency. Phull et al. [4] stated that improving cooling efficiency means decreased cooling time and increased uniformity of cooling, which is of fundamental importance in complex-shaped parts. The unevenness of temperature distribution during the injection molding process is one of the reasons that causes local shrinkage and the internal stress, which, in turn, causes the warpage of the part. Warpage is mainly determined by the cooling conditions [2]. Martinez et al. [5] showed that cooling time is one of the most significant processing parameters that influence the warpage of injection molded parts. Cooling efficiency can be enhanced through the right choice of materials, a good mold construction strategy, and the proper layout of the cooling circuit (Fig. 1).

Apart from reducing the time for mold production, AM helps to improve cooling efficiency. The spectrum of materials for additively manufactured mold inserts ranges from neat polymers to high-strength metals, depending on the required durability and thermal conductivity. The higher the thermal conductivity of the mold material, the more

* Corresponding author at: Department of Polymer Engineering, Faculty of Mechanical Engineering, Budapest University of Technology and Economics, Műegyetem rkp. 3., H-1111 Budapest, Hungary.
E-mail address: ageyevat@pt.bme.hu (T. Ageyeva).

https://doi.org/10.1016/j.jmapro.2022.07.034
Received 23 August 2021; Received in revised form 6 July 2022; Accepted 8 July 2022
Available online 25 July 2022

effective cooling is. Zink and Kovács [6] have demonstrated by simulations that even a well-designed cooling circuit is not efficient enough if the thermal conductivity of the mold material is inadequate. However, materials with high thermal conductivity are rarely used because of their limited mechanical performance and manufacturability; actual mass production must include steel because only steel can withstand more than 10^5 cycles. Among all the AM processes that can produce metal parts, powder bed fusion (PBF) is one of the most popular. This is because of the higher accuracy and better surface finish of PBF compared to other metal AM processes [7]. Also, as stated in [8], PBF is the most available system on the market. PBF systems use either an electron beam or laser to melt and fuse the metal powder together. The corresponding processes are called electron beam melting (EBM) and laser powder bed fusion (L-PBF). PBF systems are able to form metal layers with thicknesses between 20 and 60 μm [9]. Feng et al. [10] claimed that with the Powder Bed Fusion (PBF) process, inserts with conformal cooling channels could be built from steel, but some conventional methods, like casting and even machining, can also be used for these purposes. An optimal solution is combining AM and conventional machining; this combined process is known as hybrid manufacturing. Cardon et al. [11] presented that hybrid solutions with the proper combination of materials and manufacturing technologies (Fig. 2) can provide faster cooling, while preserving the mechanical performance and manufacturability of the mold.

Martinho et al. [12] showed that a hybrid mold is usually a base plate and an insert (Fig. 3). The base plate is the support structure, while the insert forms the part. The base plate is usually manufactured by conventional machining methods, while the insert is produced by AM techniques. Neither complexity nor materials are limited in the case of hybrid molds, and a wide variety of technologies can be used to manufacture durable mold inserts with excellent heat removal for injection molding.

Numerous studies are dedicated to the development of hybrid AM molds with steels and alloys of high thermal conductivity. According to Mazumder et al. [13], a mold that consists of an H13 steel insert and a heat sink made of copper reduces cycle time by 40 % compared to a mold of pure steel. Ahn and Kim [14] created a thermal management mold insert consisting of three layers made of different materials. The three materials for the mold insert were P21 tool steel in the cavity area for high strength, Ampcoloy 940 in the bottom part to dissipate the heat, and a special nickel–copper alloy as a mid-layer to decrease thermal stresses. Imran et al. [15] produced a die for high-pressure die casting, which was made from copper with a 2 mm layer of H13 tool steel deposited on it. The proposed solution reduced solidification time by up to 30–35 % compared to conventional steel dies. Reddy and Panitapu

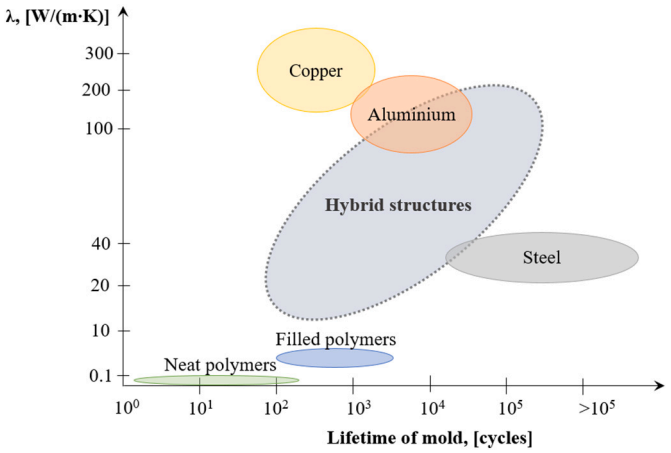

Fig. 2. Thermal and mechanical performance of different mold materials (based on [2]).

[16] examined three alternative materials for the mold insert: tool steel, copper, and beryllium-copper. They found that the beryllium-copper insert extracts heat much faster than steel or pure copper inserts. Bennett et al. [17] created a bimetallic injection mold by depositing 17–4 PH stainless steel on a copper substrate. They proved the principal possibility of producing a mold consisting of high thermal conductivity (copper) and highly wear-resistant (steel) materials. However, they did not examine the thermal properties of the new mold and did not prove its operability during injection molding.

Another approach to increase the efficiency and uniformity of cooling simultaneously is to improve the layout of the cooling circuit. Davis et al. [18] reported that with AM, it is possible to build conformal cooling channels, which can be curved and placed at an even distance from the cavity. Conformal channels can reduce cooling time by 30–40 % compared to conventional drilled channels. Kuo et al. [19] stated that the optimal distance between the wall of the conformal cooling channel and the surface of the injection mold is 2 mm in general. Contrary to this oversimplified statement, Colmenero et al. [20] presented a new design of conformal cooling channels with parametric lattice geometry, valid for any plastic part. Berger et al. [21] ran simulations for three different types of molds, and their results showed that more heat is transferred to the cooling channels if the thermal conductivity of the mold material is high, but this effect had low importance. This statement is misleading because heat transfer depends on the Reynolds number of the coolant, while heat conductivity depends on the material of the mold, but there is

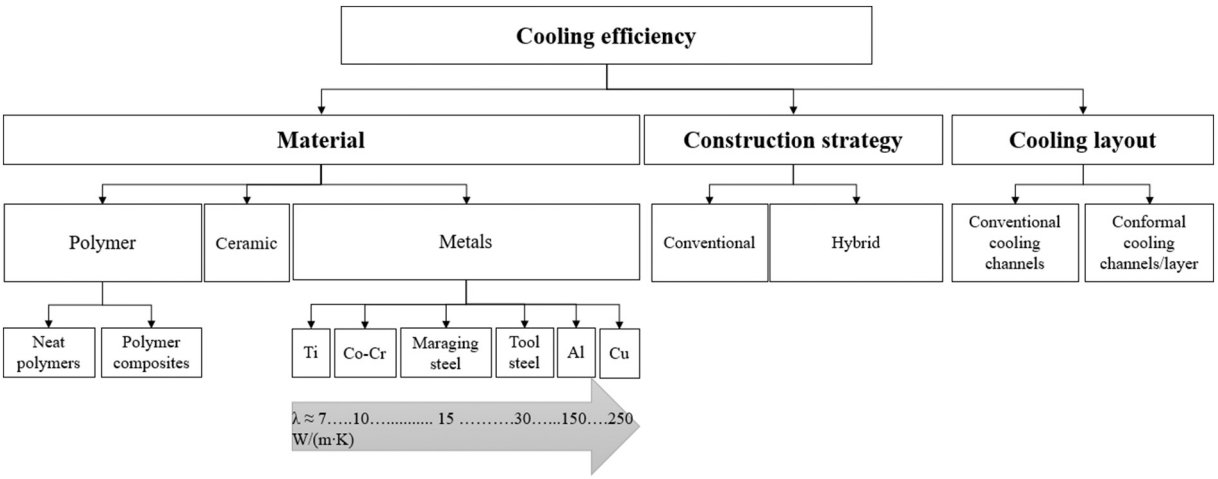

Fig. 1. Engineering approaches to increase the cooling efficiency of injection molding.

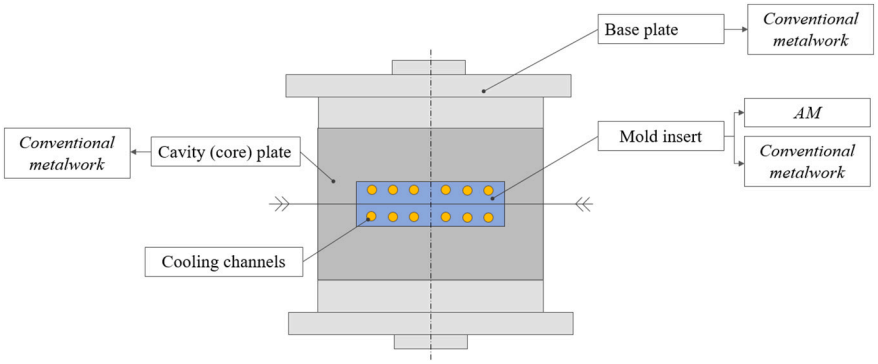

Fig. 3. The hybrid mold concept (schematically).

no direct relationship between these two. Saifullah et al. [22] simply inserted a copper tube inside the cooling channel and claimed that this bi-metallic cooling channel increases cooling efficiency. Unfortunately, they forgot to consider the change in diameter due to the extra tube, so the change in Reynolds number was not taken into account in their calculations, which led to a misleading conclusion. Park and Dang [23] improved the cooling of an industrial mold by combining conventional manufacturing with a 3D printing method. They designed the conformal cooling channels by combining analytic and simulation methods.

In this way, AM, in combination with conventional metalwork techniques, enables the creation of a cost-effective mold for mass production with high cooling efficiency. Duda and Raghavan [24] concluded that the preferred AM technique for the production of hybrid molds production is L-PBF. This technique offers the shortest manufacturing time, cost-effective assembly, and the use of a wide variety of processed metals [25,26]. Asgari and Mohammadi [26] agreed that L-PBF allows the building of complex shapes with negligible porosity and the accuracy required for molds. The most common material for L-PBF is maraging steel, which is replacing P20 and H13 tool steels. Several studies reported the successful production of mold inserts via L-PBF. Zink and Kovács [27] produced mold inserts from maraging steel (MS1) and investigated their efficiency and also the possible problems caused by limescale.

In this study, we aim to improve the cooling efficiency of a 3D-printed mold by combining copper and steel with the use of L-PBF and casting. We developed a two-cavity mold block with two inserts, one of which was entirely steel, produced by L-PBF, while the other one was a hybrid mold block made of copper and steel, produced with a hybrid procedure. First, we formed a steel shell with the conformal channels via L-PBF and then cast copper into the shell to manufacture the hybrid insert. We examined the cooling efficiency of the novel hybrid mold through the analysis of cooling uniformity, and the estimation of the optimal cooling time for each insert.

2. Materials and equipment

2.1. Materials

2.1.1. Materials for the mold

We used maraging steel 1.2709 (MS1) for the L-PBF mold insert and also for the shell of the hybrid mold insert. To cast the hybrid mold insert, we used pure copper. For the ejector pins, we used 1.2210 tool steel. The properties of the MS1 steel and copper are presented in Table 1.

2.1.2. Materials for injection molding

We used Acrylonitrile Butadiene Styrene (ABS) Terluran GP-35 (INEOS Styrolution Group GmbH, Frankfurt, Germany) for the injection molding tests (Table 2). Prior to injection molding, the material was dried in a hot-air drier (WGL-45B, Huanghua Faithful Instrument *Co.*, LTD, Huanghua, Cangzhou, China) at 80 °C for 4 h.

Table 1
Some mechanical and thermal properties of the materials used for the mold inserts.

Property	Value	
	MS1	Copper
Density, kg/m^3	8000	8930
Tensile strength, MPa	2050	210
Young modulus, GPa	180	117
Thermal conductivity at 20 °C, W/(m•K)	20	386–390
Specific heat capacity, J/(kg•K)	450	380
Coefficient of linear thermal expansion at 20 °C, 10^{-6}/K	10.3	17.5

Table 2
Some properties of ABS used for the injection molding tests.

Property	Value
Density, kg/m^3	1040
Melt temperature range, °C	220–260
Mold temperature range, °C	30–80
Recommended ejection temperature, °C	84
Melt volume rate at 220 °C, cm^3/10 min	34

2.2. Equipment and process parameters

2.2.1. Manufacturing the mold inserts and quality control

For the production of the L-PBF mold inserts, we used EOS M270 equipment (EOS GmbH., Krailling, Germany), with 200 W laser power, 20 μm powder layer thickness, and alternating beam scanning strategy in a nitrogen atmosphere. In order to increase the hardness and strength of the developed mold inserts, we also performed heat treatment in a Denkal 6B (Kalória Hőtechnikai Kft., Budapest, Hungary) oven by age hardening at 500 °C for 3 h in air.

For quality control purposes, we examined the volumetric porosity of the hybrid mold insert by Computer Tomography (Yxlon Modular, YXLON, Hamburg, Germany). The prepared inserts were scanned with a tube voltage of 450 kV and a tube current of 1.55 mA with a focal spot of 0.4 mm. A line detector was used to capture the projections in order to minimize noise from scattered X-rays. 1440 projections were taken of the insert with around 5 times magnification, resulting in a voxel size of 0.08 mm. The reconstructed slices were loaded into a CT data analysis software (VGStudio MAX 2.2, Volume Graphics GmbH, Heidelberg, Germany) to quantify the porosity of the insert.

An optical microscope (Zeiss Axio Imager M1, Carl Zeiss AG, Oberkochen, Germany) was used to inspect the copper–steel interface for porosity.

We used numerical simulations to evaluate the thermal properties of the hybrid mold insert, taking into account real porosity and porosity

distribution.

2.2.2. Injection molding machine and process parameters

We produced the specimens on an Arburg Allrounder 270S 400-170 advanced (ARBURG Holding GmbH, Lossburg, Germany) injection molding machine. Mold temperature was 40 °C, melt temperature was 250 °C, injection volume was 45 cm^3, injection rate was 30 cm^3/s, switchover volume was 8 cm^3, clamping force was 40 t, the pressure limit was 960 bar, holding pressure was 500 bar, and holding time was 3 s. We varied residual cooling time from 0 s to 40 s in 5 s steps.

2.2.3. Equipment for temperature measurement

To evaluate the cooling efficiency of the studied inserts, we measured the temperature of the surface of the specimens at the moment of ejection by infrared thermography (IRT). We used an infrared camera Flir 325SC (FLIR Systems, Inc., Wilsonville, USA).

2.2.4. Equipment for warpage measurement

We characterized the deformation of the parts with the Atos Core Optical 3D-scanner (GOM GmbH, Braunschweig, Germany).

2.2.5. Numerical simulations

The simulations were conducted with the Autodesk Simulation Moldflow Insight 2021. Each mold insert was modeled in individual models. We used four-node tetrahedral elements for meshing in the entire model. Global element size was set to 2.5 mm, but mesh size was changed to 1.5 mm in complex areas, like conformal cooling channels. The total number of elements was nearly 3.2 million for each model. We used Cool FEM method with the conduction solver for thermal analysis. This provides options to investigate the transient state of the mold. A conduction solver was used for the cooling calculations. Minor losses and friction in the cooling channels were included in the calculations. Perfect clamping was assumed; therefore mold block conductance was set to the default 30,000 W/(m^2K) (Table 3). Coolant flow rate and initial mold insert temperature were chosen (2.8 l/min and 42 °C, respectively) according to the results. The software considers the pressure dependency of the heat transfer coefficient (HTC) between the melt and the mold with three different values for filling, holding, and cooling. Based on preliminary simulation results, we set the HTC values to 5000 W/(m^2K), 500 W/(m^2K) and 10 W/(m^2K), respectively.

3. Mold and method development

3.1. Hybrid insert development

We produced two mold inserts for a specimen with a simple geometry. The specimen consisted of two 75 mm × 65 mm × 2 mm sheets. The angle between the two sheets is 90°, so the total height of the specimen is 32.5 mm. Both of them included the same longitudinal conformal cooling channels. However, the materials used for the manufacturing of mold inserts were different. Thus, one of the inserts was produced entirely from maraging steel by L-PBF. This insert is considered the reference, and hereafter we will call it "L-PBF insert" (Fig. 4). The second insert consists of maraging steel and copper. First, a steel shell with conformal cooling channels was produced by L-PBF. The thickness of the wall of the shell and of the conformal channels was 0.8 mm. The internal diameter of the conformal channels was 5 mm. The steel shell was then filled with molten copper, thus a hybrid structure was formed. Hereafter, we will call this insert "hybrid insert". The design of the hybrid mold insert we developed is presented in Fig. 5.

Table 3
Some parameters of the simulation of injection molding.

Parameter	Value
Ambient temperature, °C	25
Mold surface temperature, °C	40
Initial mold temperature, °C	40
Coolant flow rate, l/min	2.8
Mold block conductance, W/(m^2K)	30,000
Number of heat flux time steps	25
Transient mold temperature convergence tolerance, °C	0.1
Maximum number of transient mold temperature cycles	250

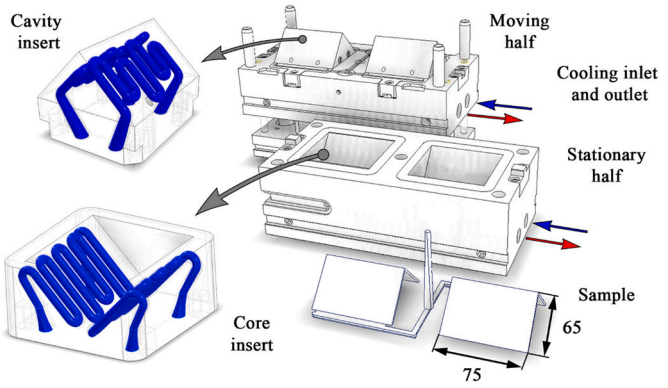

Fig. 4. The design of the mold and its cooling circuit.

3.2. Development of the method to evaluate the efficiency of the insert

In this study, under the term "insert efficiency", we understand the heat removal capability of each insert and the uniformity of the temperature field distribution on the surface of the part.

We compared the heat removal capabilities of L-PBF and hybrid inserts by calculating the relative difference in heat removal (1):

$$\xi = \frac{Q_{hybrid}^{cooling} - Q_{L-PBF}^{cooling}}{Q_{hybrid}^{cooling}} \bullet 100\%, \quad (1)$$

where $Q_{L-PBF}^{cooling}$ and $Q_{hybrid}^{cooling}$ are the amounts of heat removed through the cooling channels during the molding cycle by the L-PBF and hybrid insert, respectively (J). The heat values were evaluated with the simulation.

The temperature field distribution characterizes insert efficiency only implicitly. The unevenness of temperature distribution during cooling causes warpage of the injection molded part. Consequently, the analysis of warpage helps to compare the efficiency of different mold inserts.

To characterize the efficiency of the studied mold inserts, we conducted the measurement and simulation of temperature fields on the surface of the injection molded part as well as the measurement of warpage.

3.2.1. Infrared thermography for mold efficiency analysis

The layout of the IRT experimental setup is presented in Fig. 6.

We maximized the emissivity of the mold insert with black spray paint. The resulting emissivity of the mold inserts was 0.95. The

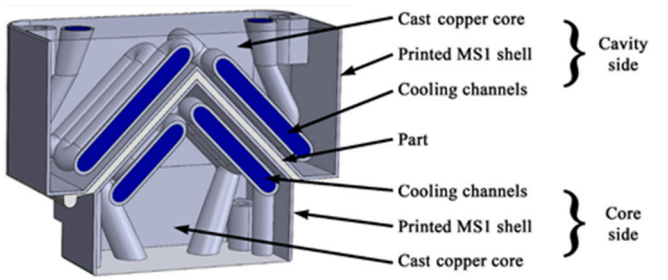

Fig. 5. The structure of the hybrid insert.

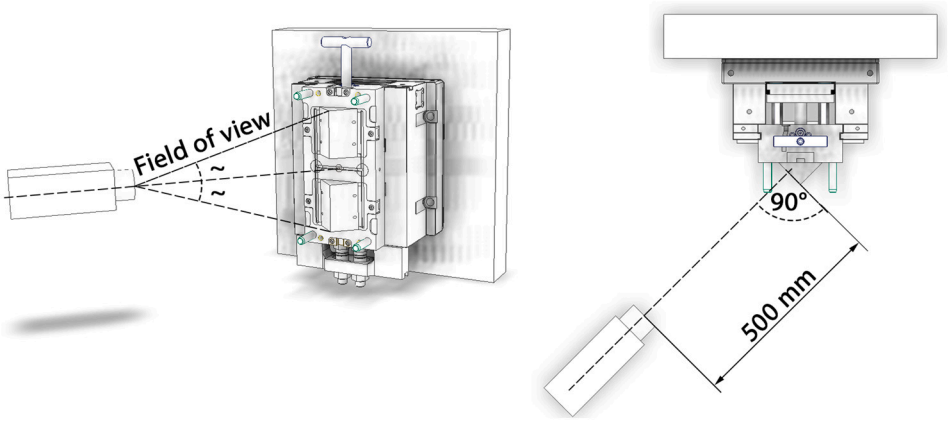

Fig. 6. Thermal measurements set up.

reflected apparent temperature was found to be $T_{refl} = 27.4$ °C.

To measure the equilibrium thermal state of the mold, we started the temperature measurements after fifty cycles of injection molding. The typical image of temperature distribution on the surface of the parts is shown in Fig. 7. The temperature distribution of the surface is even in the case of booth inserts, but small differences can be seen in the region of the ejector pins. In the case of the L-PBF insert, the region of the ejector pins has lower temperature because the insert has lower cooling efficiency than the pins. The hybrid insert is more thermally efficient than the ejector pins and therefore the temperature is slightly higher in the region of the pins than on the surface of the part.

3.2.2. *Development of a method for warpage analysis*

To characterize the deformation of the produced parts, we used 3D-scanning. We digitized the surface of each part right after the demolding. As a result of scanning, we obtained a raw cloud of points with high resolution, which described the surface of the part. To process 3D-scanned data, we first assigned a coordinate system (*XYZ*) to the part. The origin of the coordinate system was at one of the part's corners, while the *X*-axis coincided with the edge of the rooftop part. The *XY* and the *XZ* plane coincided with the faces of the part (Fig. 8a). Therefore, we used the X-axis to characterize the warpage of the parts.

We decomposed the 3D-scanned image of the part into two halves, where each half was one of the faces. We analyzed the deformation of a part with an angle between the faces of the part. We found that this angle changes along the *X*-axis; therefore, we evaluated this angle at different coordinates along the *X*-axis. We distinguished 19 positions along the X-axis (Fig. 8a) and fitted planes onto the separated halves in each position. For plane fitting, we used only the points whose *X* coordinates were in the range of ±3 mm from a certain position (Fig. 8b).

A typical image of the relation between the calculated angles and the *X* coordinate is presented in Fig. 8c. We repeated this evaluation procedure for all the parts produced with the L-PBF and hybrid inserts with all different residual cooling times specified in Section 2.2.2. In Fig. 8d, a 3D diagram illustrates the relation between the angle at the part faces, the *X* coordinate (part edge), and residual cooling time.

The designed and desired angle between the part faces is 90°. The deviation from this angle means either "opening" or "closing" of the angle, which we refer to as "angle deformation". The alteration of the angles along the edge of the part means that the faces themselves deformed, which we call "plane deformation".

4. Results and discussion

4.1. *Hybrid mold insert examination*

First, we examined the interface between steel and copper in the hybrid insert by optical microscopy. The analysis of the micrographs of polished cross-sections shows a continuous and deep diffusion of copper into the grain boundaries of steel (Fig. 9). This diffusion interface provides good mechanical adhesion between the two materials. Furthermore, no oxidation can be observed in the interface layer, which results in good thermal conductivity.

The typical defects that can appear during casting are cavities and

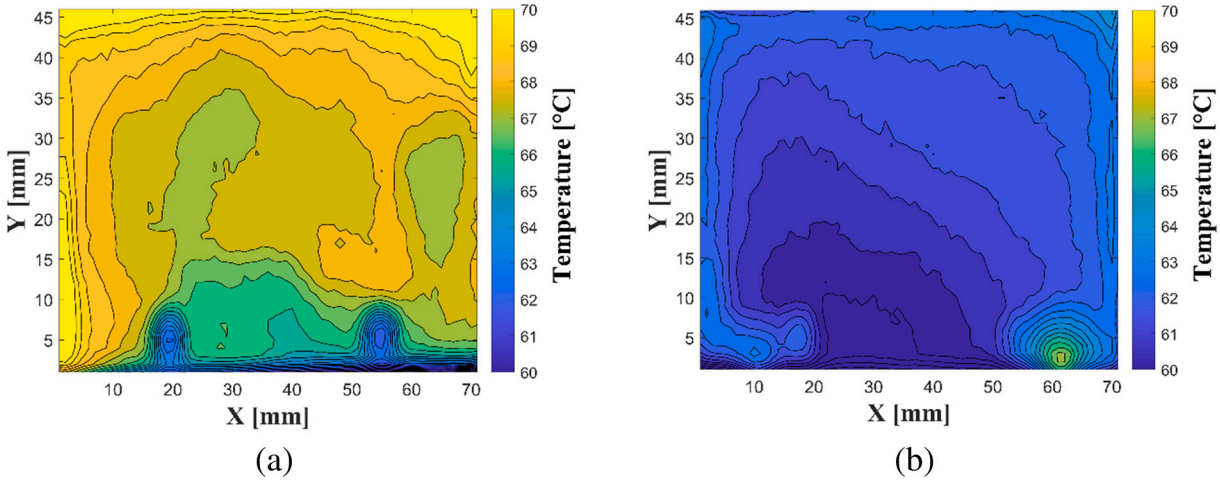

Fig. 7. A typical image of temperature distribution of the surface of a part produced with (a) L-PBF and (b) hybrid insert.

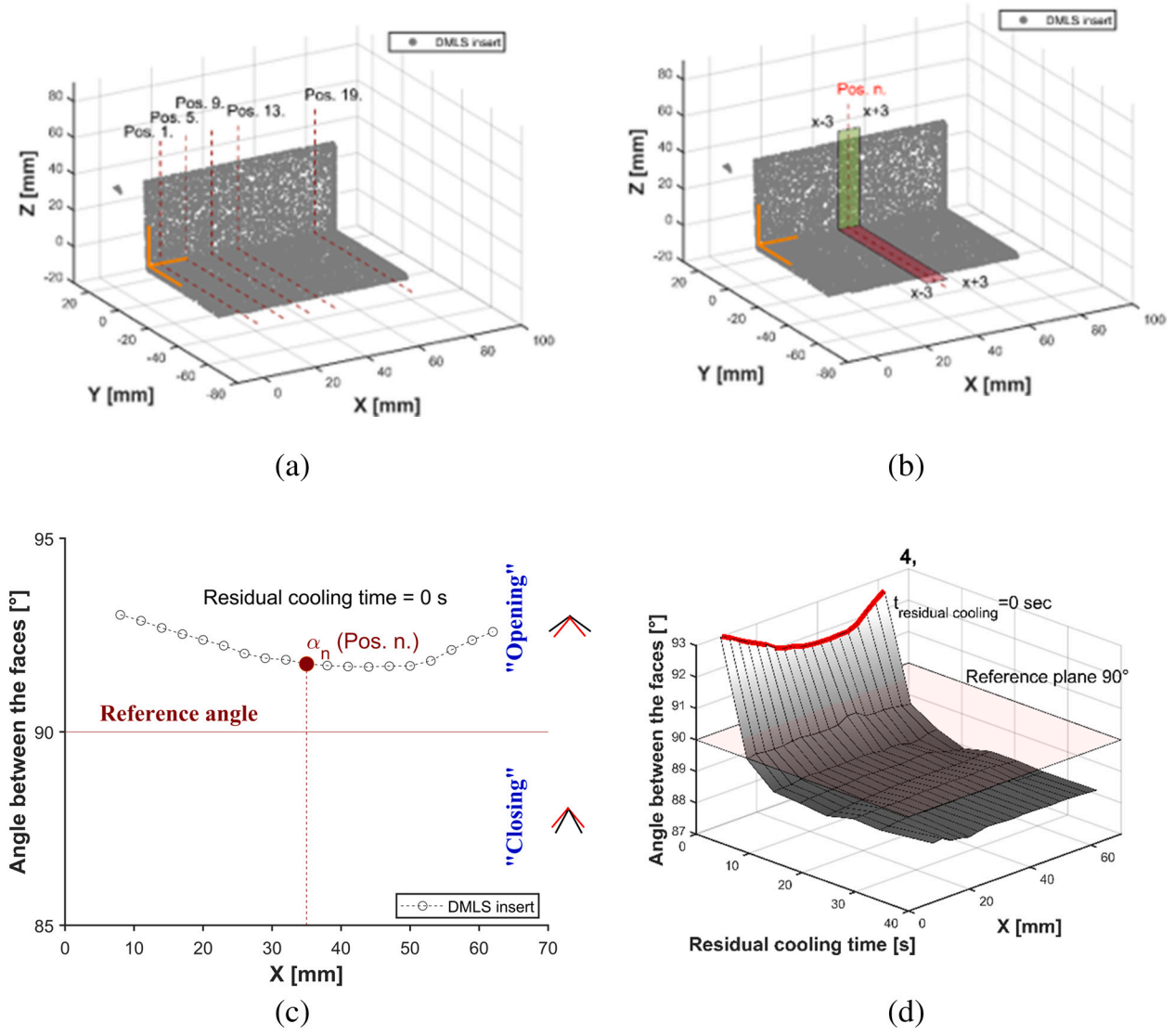

Fig. 8. The steps of warpage evaluation: (a) Oriented 3D-scanned data (cloud of points); (b) separated cloud of points and planes fitted on the face segments; (c) typical image of the distribution of the angle between the faces of the part along the *X*-axis (for the residual cooling time equal to zero); (d) the relation between an angle of the part faces, the *X* coordinate and residual cooling time.

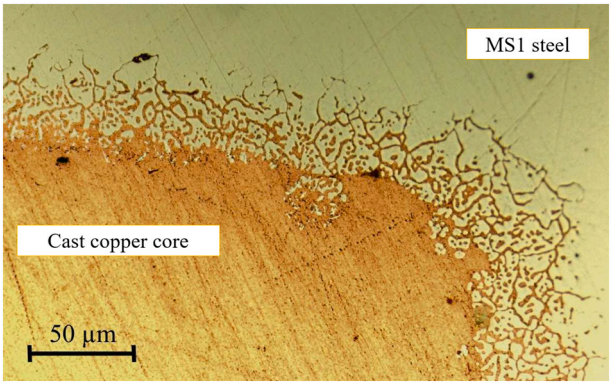

Fig. 9. The microscopic image of the polished sample showing the porosity at the copper–steel interface in the hybrid insert.

cracks. These defects decrease the thermal conductivity of the final part, which is undesirable in the case of a mold insert. That is why we examined the porosity of the cast part of the hybrid insert with CT. We analyzed the reconstructed CT data of the mold to measure porosity. We only analyzed the volumes of the copper since the steel parts can be considered solid. The stationary half of the hybrid mold contained 234,969 mm^3 of copper, of which 357 mm^3 was void, resulting in a porosity of 0.152 %. The stationary mold contained 47 individual voids, ranging from 1.2 mm to 11.8 mm in diameter, with an average void diameter of 3.0 mm. The moving half of the hybrid mold contained 140,813 mm^3 of copper, of which 1979 mm^3 was void, resulting in a porosity of 1.405 %. The moving mold contained 234 individual voids, ranging from 1.0 mm to 15.7 mm in diameter, with an average void diameter of 2.6 mm. We used the CT scan of the mold insert to create a numerical model, which includes pores (Fig. 10).

4.2. Optimization of the injection molding process

For the optimization of the injection molding cycle, it is important to define a minimum required value of holding time. A holding phase is used to compensate for the unwanted deformation that can occur due to the decrease of the specific volume of the polymer melt during cooling. The moment in the cycle when the gates freeze and it is not possible to push more material into the mold cavity is considered the end of the

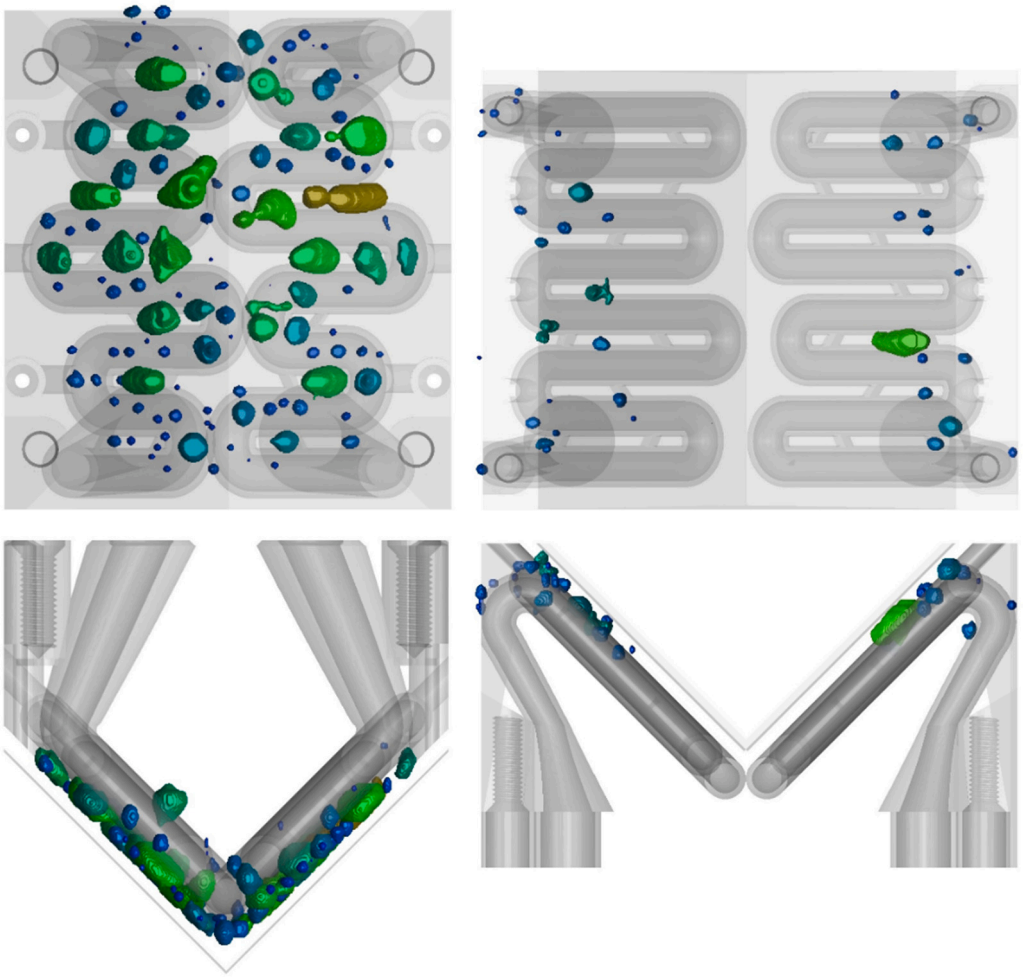

Fig. 10. 3D scan of the hybrid insert, which shows the volume and distribution of the pores.

holding phase. Even though the physics of this process is clear, it is quite difficult to determine the optimum holding time in practice. Usually, holding time is determined by trial and error, which depends on the operator's experience. In this study, we propose a universal method, which allows a more precise calculation of holding time.

To calculate the gate freeze time, we measured the weight of the parts produced with different holding times. The weight of the parts increased with increasing holding time, until the gates froze off. Holding time was varied from 0 to 8 s in 0.5 s steps. A saturation curve can be fitted on the obtained weight data (Fig. 11); this curve can be approximated with an asymptotic regression model. This model is also known as

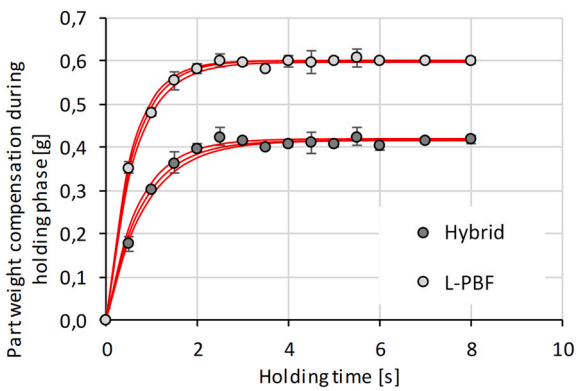

Fig. 11. The saturation curves fitted to the empirical data.

the Mitscherlich law. We modified the Mitscherlich law to describe our specific measurement data (2):

$$m\left(t_{holding}\right) = m_{\infty} - \left(m_{\infty} - m_0\right)e^{-\frac{t_{holding}}{\tau}} \tag{2}$$

where m_{∞} is the maximum achievable weight of a part (kg); m_0 is the weight of a part without a holding phase (kg); $t_{holding}$ is the holding time (s), and τ is a time constant (s). The values of m_{∞} and m_0 can be measured, therefore only the time constant τ has to be calculated. We fitted Eq. (1) to the empirical data (Fig. 11) and defined the τ time parameter for both mold inserts.

Knowing all the parameters of Eq. (2) (m_0, m_{∞}, τ), we can calculate the holding time, which is needed to reach a saturation level of 95 %, which corresponds to 95 % of the maximum possible weight of the part. We call this time $t_{hold}^{0.95}$ and we consider this time the gate freeze time. We found that in the case of the L-PBF insert, $t_{hold}^{0.95}$ was equal to 2.04 s, while in the case of the hybrid insert, it was 2.71 s. This difference between the $t_{hold}^{0.95}$ of the two inserts might be caused either by the differences in the sizes of cavities or the thermal differences of the two inserts. For further investigation, we used 3 s as holding time, which is long enough to compensate for the shrinkage in the case of both inserts. Therefore, we can compare the deformation of the parts caused by cooling without the influence of the amount of compensation.

We performed injection molding and measured the actual cycle parameters. The longest investigated injection molding cycle is presented in Fig. 12.

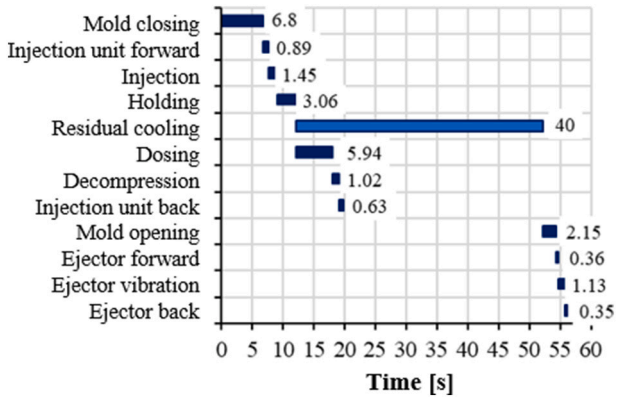

Fig. 12. The longest investigated injection molding cycle with 40 s residual cooling.

4.3. Evaluation of the efficiency of the prototype mold inserts

4.3.1. The results of thermal measurement and simulation

4.3.1.1. Step 1: evaluation of the efficiency of the inserts. We used Cool FEM simulation to evaluate the efficiency of the inserts. However, to prove the validity of the conducted simulation, we first verified it with experiments. Since the complex cooling channels are located near the cavity, thermocouples cannot be used. Thus, we measured the temperature of the surface of the part at the moment of ejection by IRT and compared the results with the corresponding simulation results. We found a good correlation between the measured and simulated temperature fields (Fig. 13). The correlation coefficient of the measured and calculated temperature fields was 0.995 and 0.986 for the L-PBF and hybrid inserts, respectively. The biggest difference between the measured and simulated results was at the corners of the part and near the ejector pins for both mold inserts (Fig. 13). Due to the good correlation, we used the calculated thermal results for the further evaluation of the heat removal capability of each insert, and the evaluation of residual cooling time. For further comparison, we calculated the measured and simulated average temperatures of the part surface (T_{av}^{IRT} and T_{av}^{sim}, respectively). The difference between T_{av}^{IRT} and T_{av}^{sim} never exceed 5 °C.

Heat removal of the cooling channels was calculated based on the simulations, which calculated the average heat flux, which was then multiplied by the appropriate cycle time. The cooling channels of the hybrid insert can remove more heat than the circuits of the L-PBF insert for all residual cooling times (Fig. 14). This can be explained by the higher thermal conductivity of the hybrid mold insert, because energy is transferred faster to the cooling channels, thus the cooling channels can remove more energy in a certain time interval.

We calculated the relative difference in heat removal of the L-PBF and hybrid inserts with Eq. (1), for which we used the values of the parameters ($Q_{L-PBF}^{cooling}$ and $Q_{hybrid}^{cooling}$) obtained with the simulation. We did this calculation for different residual cooling times ranging from 0 to 40 s. For all the examined values of residual cooling time, the hybrid insert demonstrated 10–15 % higher heat removal than the L-PBF mold insert. The results of the calculation of relative cooling efficacy are presented in Fig. 15.

4.3.1.2. Step 2: analysis of the effect of porosity on the thermal properties of the hybrid mold insert. We analyzed and evaluated the effect of porosity on the cooling efficiency of the hybrid mold insert. We simulated all the injection molding cycles mentioned in Section 2.2.2, using the idealized model of the hybrid insert and the realistic model, which contains voids.

The comparison analysis showed that the maximum difference between the average temperatures for the idealized model and the model with voids does not exceed 0.27 °C in the case of zero residual cooling time. When residual cooling time was longer than zero, the difference between the temperatures was even less. Therefore, we concluded that the influence of the pores in the hybrid insert is negligible on the temperature of the injection molded part. Consequently, we can use the

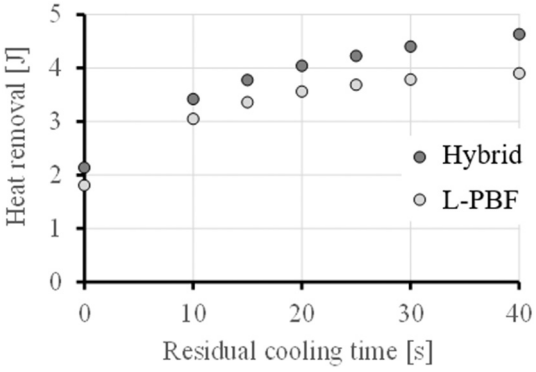

Fig. 14. Heat removal of the cooling channels of the L-PBF and the hybrid inserts.

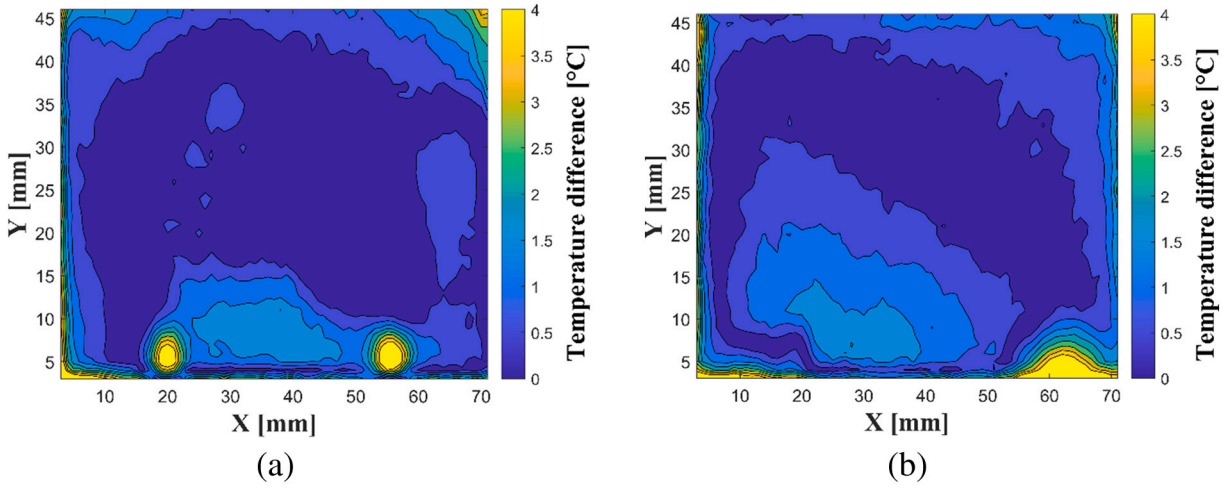

Fig. 13. The difference between the temperature field distributions obtained with the simulation and by IRT (at the moment of part ejection): (a) for the L-PBF insert; (b) for the hybrid insert.

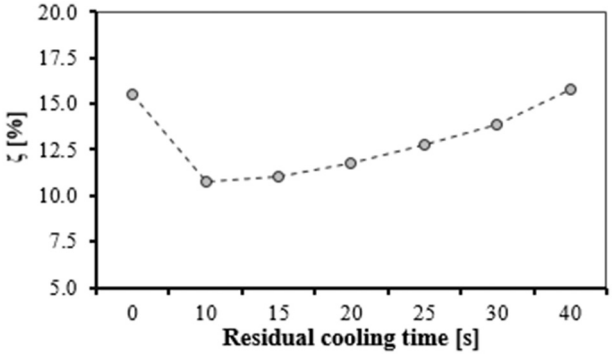

Fig. 15. The relative difference in heat removal of the two mold inserts (based on Eq. (1)).

idealized model for further simulations.

4.3.2. Step 3: evaluation of the temperature-based results

The measured average part surface temperatures (T_{av}^{IRT}) and their standard deviations (SDT) also characterize the cooling efficiency of mold inserts at different cooling times (Fig. 16). Thus, when the residual cooling time is in the range of 0 to 10 s, T_{av}^{IRT} for the hybrid insert is approximately 5 °C lower than the same parameter for the L-PBF insert, which leads to a shorter cycle time. Moreover, in the examined range of residual cooling time, the SDT of T_{av}^{IRT} is lower for the hybrid insert than for the L-PBF insert. Lower SDT in this case, means more uniform heat extraction. For residual cooling times ranging from 10 to 20 s, the difference between T_{av}^{IRT} obtained for both inserts steadily decreases. For residual cooling times exceeding 20 s, the difference between the T_{av}^{IRT} of the L-PBF and hybrid mold inserts is negligible.

The residual cooling time can be calculated with transient thermal simulation. The residual cooling time is when the center of the part reaches the ejection temperature, which is 84 °C for the ABS we used. We found that in the case of the L-PBF mold insert, the residual cooling time was 6.1 s, while in the case of the hybrid insert, it was 5.2 s, almost 15 % lower than for the L-PBF insert. A reduction in the residual cooling time means a reduction of total cycle time, which is an important improvement.

4.3.3. The results of warpage measurement

We examined the effect of cooling time on the angle and plane deformation of the parts produced. We also calculated the deformation which is the difference from the reference 90°, for the optimal cooling time. We used linear interpolation in the calculations. A comparison of the results of the two inserts (Fig. 17) shows that angle deformation is positive ("opening") for both inserts when no residual cooling is used. As

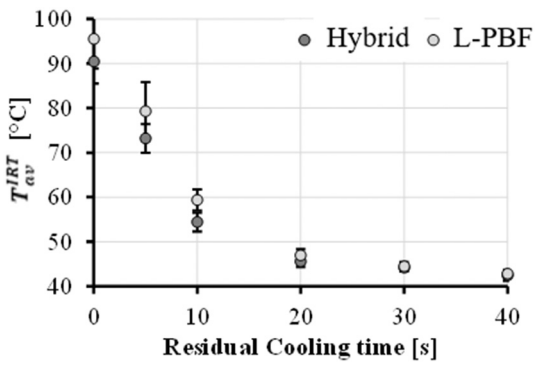

Fig. 16. T_{av}^{IRT} and its SDT for the L-PBF and hybrid mold inserts at different residual cooling times.

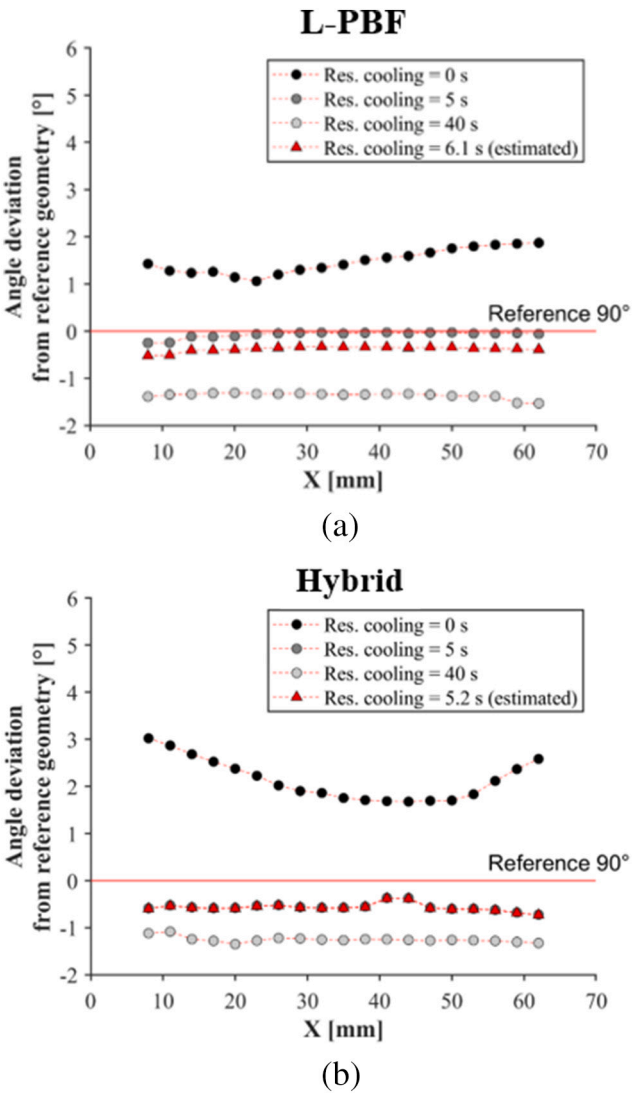

Fig. 17. Angle deviation from the reference geometry: (a) L-PBF; (b) hybrid mold insert.

residual cooling time increases angle deformation gets smaller, and after a point it becomes negative ("closing"). Angle deformation and its change depend on the heat removal of the inserts. The angle deformation curves of the L-PBF insert, which has lower heat removal (Fig. 14), are closer to each other than those of the hybrid insert. This means that angle deformation changes less when residual cooling time increases.

In the case of the optimal cooling time, which is based on the residual cooling time calculations, the parts showed the same small deformation regardless of which inserts they were produced in (Fig. 17 – red curves). The difference in deformation is insignificant, unlike the time required to reach the ejection temperature. The residual cooling time is significantly shorter for the hybrid insert, which means a shorter cycle time. We also calculated a theoretical residual cooling time, where deformation is minimal. The required cooling times were 4.76 s and 3.98 s for the L-PBF and the hybrid inserts, respectively. Since these residual cooling times are shorter than the time required to reach the ejection temperature, extra deformation can appear as the cross-section of the part is not fully solidified. But again, the cycle time with the hybrid mold insert is significantly shorter than with the L-PBF insert.

5. Conclusions

We developed and produced a hybrid mold insert with improved cooling. We coupled copper and steel with the use of L-PDF and casting to produce the hybrid insert. We found that the hybrid insert exhibits higher efficiency than the L-PBF insert. Our main results are the following:

1. We proved with simulation that the influence of technological defects (voids), which occur during casting, is negligible on the thermal properties of the hybrid mold insert. We also validated the simulation by IRT and found a good correlation between the calculated and measured results.

2. We proposed a method to accurately calculate optimal holding time. Based on this evaluation, we used a slightly longer holding time (3 s) than the calculated optimum to assure that the specific volume change is compensated for as much as possible with the holding phase.

3. The hybrid mold insert had a lower minimum residual cooling time (5.2 s) for ABS than the L-PBF insert (6.1 s), which is a 15 % improvement.

4. The hybrid mold insert allowed more uniform heat extraction than the reference L-PBF insert for all the examined residual cooling times.

5. We showed that the parts produced with the L-PBF and hybrid mold inserts have almost the same deformation. However, cooling time (and therefore cycle time) can be 0.9 s shorter if the hybrid mold insert is used, which is a considerable improvement for mass production.

We plan to continue this research and our plan is to decrease the porosity of the inserts, and to optimize the manufacturing process of the hybrid mold production. The formation of the steel shell can be optimized to reduce the weight of the maraging steel used, which will increase the ratio of copper, and thus the overall thermal conductivity of the insert.

Funding

This work was supported by the National Research, Development and Innovation Office, Hungary (2019-1.1.1-PIACI-KFI-2019-00205, 2018-1.3.1-VKE-2018-00001, 2017-2.3.7-TÉT-IN-2017-00049). The research reported in this paper was supported by the BME NC TKP2020 grant of NKFIH Hungary. The research was done under the scope of the Project no. RRF-2.3.1-21-2022-00009, etitled “National Laboratory for Renewable Energy” which has been implemented with the support provided by the Recovery and Resilience Facility of the European Union within the framework of Programme Széchenyi Plan Plus.

CRediT authorship contribution statement

Dániel Török: Performing Experiments, Data analysis and interpretation, Writing. **Béla Zink:** Performing Experiments, Simulation. **Tatyana Ageyeva:** Conceptualization, Writing, Review & Editing. **István Hatos:** Performing Experiments. **Martin Zobač:** Mold Production. **Imre Fekete:** Performing Experiments **Róbert Boros:** 3D design, mold design **Hajnalka Hargitai:** Supervision. **József Gábor Kovács:** Supervision, Conceptualization, Review & Editing.

Declaration of competing interest

The authors declare that they have no known competing financial interests or personal relationships that could have appeared to influence the work reported in this paper.

Acknowledgments

We wish to thank ARBURG HUNGÁRIA KFT. for the ARBURG Allrounder 370S 700-290 injection molding machine, TOOL-TEMP HUNGÁRIA KFT., LENZKES GMBH and PIOVAN HUNGARY KFT. for the accessories.

References

[1] León-Cabezas MA, Martínez-García A, Varela-Gandía FJ. Innovative advances in additive manufactured moulds for short plastic injection series. Procedia Manuf 2017;13:732–7. https://doi.org/10.1016/j.promfg.2017.09.124.
[2] Bagalkot A, Pons D, Clucas D, Symons D. A methodology for setting the injection moulding process parameters for polymer rapid tooling inserts. Rapid Prototyp J 2019;25:1493–505. https://doi.org/10.1108/RPJ-10-2017-0217.
[3] Galizia FG, ElMaraghy W, ElMaraghy H, Bortolini M, Mora C. The evolution of molds in manufacturing: from rigid to flexible. Procedia Manuf 2019;33:319–26. https://doi.org/10.1016/j.promfg.2019.04.039.
[4] Phull GS, Kumar S, Walia RS. Conformal cooling for molds produced by additive manufacturing: a review. Int J Mech Eng Technol 2018;9:1162–72.
[5] Sánchez R, Aisa J, Martinez A, Mercado D. On the relationship between cooling setup and warpage in injection molding. Mesurement 2012;45:1051–6. https://doi.org/10.1016/j.measurement.2012.01.039.
[6] Zink B, Kovács JG. Enhancing thermal simulations for prototype molds. Period Polytech Mech Eng 2018;62:320–5. https://doi.org/10.3311/PPme.12526.
[7] Khorasani A, Gibson I, Veetil JK, Ghasemi AH. A review of technological improvements in laser-based powder bed fusion of metal printers. Int J Adv Manuf Technol 2020;108:191–209. https://doi.org/10.1007/s00170-020-05361-3.
[8] Cooke S, Ahmadi K, Willerth S, Herring R. Metal additive manufacturing: technology, metallurgy and modelling. J Manuf Process 2020;57:978–1003. https://doi.org/10.1016/j.jmapro.2020.07.025.
[9] Murr LE, Gaytan SM, Ramirez DA, Martinez E, Hernandez J, Amato KN, Shindo PW, Medina FR, Wicker RB. Metal fabrication by additive manufacturing using laser and electron beam melting technologies. J Mater Sci Technol 2012;28:1–14. https://doi.org/10.1016/s1005- 0302(12)60016-4.
[10] Feng S, Kamat AM, Pei Y. Design and fabrication of conformal cooling channels in molds: review and progress updates. Int J Heat Mass Transf 2021;171:121082. https://doi.org/10.1016/j.ijheatmasstransfer.2021.121082.
[11] Cardon L, Houtekier R, Ragaert K, Moerman M. The effect of the mould material selection and production methodology on the thermal behaviour and tribology of injection moulds. In: al. PJBe, editor. 3rd international conference on Advanced Research in Virtual and Rapid Prototyping, Leiria, Portugal, 24-29 September. Leiria, Portugal: Taylor & Francis Group; 2007. p. 425–9.
[12] Martinho PG, Bartolo PJ, Pouzada AS. Hybrid moulds: effect of the moulding blockson the morphology and dimensional properties. Rapid Prototyp J 2009;15:71–82. https://doi.org/10.1108/13552540910925081.
[13] Mazumder J, Dutta D, Kikuchi N, Ghosh A. Closed loop direct metal deposition: art to part. Opt Lasers Eng 2000;34:397–414. https://doi.org/10.1016/S0143-8166(00)00072-5.
[14] Ahn D-G, Kim H-W. Study on the manufacture of a thermal management mould with three different materials using a direct metal tooling rapid tooling process. Proc IMechE Part B: J Eng Manuf 2009;224:385–402. https://doi.org/10.1243/09544054JEM1523.
[15] Imran MK, Masood SH, Brandt M. Bimetallic dies with direct metal-deposited steel on moldmax for high-pressure die casting application. Int J Adv Manuf Technol 2011;52:855–63. https://doi.org/10.1007/s00170-010-2783-3.
[16] Prashanth Reddy K, Panitapu B. High thermal conductivity mould insert materials for cooling time reduction in thermoplastic injection moulds. Mater Today Proc 2017;4:519–26. https://doi.org/10.1016/j.matpr.2017.01.052.
[17] Bennett JL, Liao H, Buergel T, Hyatt G, Ehmann K, Cao J. Towards bi-metallic injection molds by directed energy deposition. Manuf Lett 2021;27:78–81. https://doi.org/10.1016/j.mfglet.2021.01.001.
[18] Davis W, Lunetto V, Priarone PC, Centea D, Settineri L. An appraisal on the sustainability payback of additively manufactured molds with conformal cooling. Procedia CIRP 2020;90:516–21. https://doi.org/10.1016/j.procir.2020.01.064.
[19] Kuo C-C, Jiang Z-F, Lee J-H. Effects of cooling time of molded parts on rapid injection molds with different layouts and surface roughness of conformal cooling channels. Int J Adv Manuf Technol 2019;103:2169–82. https://doi.org/10.1007/s00170-019-03694-2.
[20] Mercado-Colmenero JM, Martin-Doñate C, Rodriguez-Santiago M, Moral-Pulido F, Rubio-Paramio MA. A new conformal cooling lattice design procedure for injection molding applications based on expert algorithms. Int J Adv Manuf Technol 2019;102:1719–46. https://doi.org/10.1007/s00170-018-03235-3.
[21] Berger GR, Zorn D, Friesenbichler W, Bevc F, Bodor CJ. Efficient cooling of hot spots in injection molding. A biomimetic cooling channel versus a heat-conductive

mold material and a heat conductive plastics. Polym Eng Sci 2019;59:E180–8. https://doi.org/10.1002/pen.25024.
[22] Saifullah ABM, Masood SH, Sbarski I. Thermal–structural analysis of bi-metallic conformal cooling for injection moulds. Int J Adv Manuf Technol 2012;62:123–33. https://doi.org/10.1007/s00170-011-3805-5.
[23] Park H-S, Dang X-P. Development of a smart plastic injection mold with conformal cooling channels. Procedia Manuf 2017;10:48–59. https://doi.org/10.1016/j.promfg.2017.07.020.
[24] Duda T, Raghavan LV. 3d metal printing technology: the need to re-invent design practice. AI Soc 2018;33:241–52. https://doi.org/10.1007/s00146-018-0809-9.
[25] Keresztes Z, Pammer D, Szabo PJ. EBSD examination of argon ion bombarded Ti-6Al-4V samples produced with DMLS technology. Period Polytech Mech Eng 2019;63:195–200. https://doi.org/10.3311/PPme.13821.
[26] Asgari H, Mohammadi M. Microstructure and mechanical properties of stainless steel cx manufactured by direct metal laser sintering. Mater Sci Eng A 2018;709:82–9. https://doi.org/10.1016/j.msea.2017.10.045.
[27] Zink B, Kovács JG. The effect of limescale on heat transfer in injection molding. Int Commun Heat Mass Transf 2017;86:101–7. https://doi.org/10.1016/j.icheatmasstransfer.2017.05.018.